ROYAL SOCIETY
OF CHEMISTRY

Check for updates

Advances in the direct electro-conversion of captured CO_2 into valuable products

Kezia Langie,†[ab] Gwangsu Bak,†[c] Ung Lee, [ID][ade] Dong Ki Lee, [ID][aef] Chan Woo Lee, [ID][b] Yun Jeong Hwang [ID] *[cg] and Da Hye Won [ID] *[adh]

The direct electrochemical conversion of captured CO_2 (capt-eCO_2R) into valuable chemicals has recently emerged as a promising carbon capture and utilisation technology that will contribute to achieving net-zero carbon emissions. Conventional electrochemical CO_2 (eCO_2R) typically uses pure CO_2 gas as a reactant; thus, this system requires substantial energy and capital allocation across the entire process, from the initial CO_2 capture to the post-CO_2 conditioning for product separation. The capt-eCO_2R addresses these limitations and presents a compelling economic advantage by integrating the CO_2 capture and direct electro-conversion of captured CO_2 in the form of carbamate and (bi)carbonate without a CO_2 conditioning process. The capt-eCO_2R is still in the early stages of development and is not as mature as the conventional eCO_2R; thus, several challenges remain to be addressed to improve system performance. This review provides a comprehensive overview of the capt-eCO_2R system, including various system configurations, suitable catalysts, and strategies to enhance performance within captured media. The reaction mechanisms depend on the form of captured CO_2; therefore, we categorised them according to the type of CO_2 absorbent. The outlook, ongoing challenges, and strategies for future development are also presented.

1. Introduction

The concentration of CO_2 in the atmosphere has increased over hundreds of years owing to anthropological activities, reaching 413.2 ppm in 2020, which represents an increase higher than the average growth rate observed over the past decade (2.5 ppm per year).[1] Carbon capture, utilisation, and storage (CCUS) technology has attracted considerable interest as a means to overcome the climate crisis caused by CO_2.[2–4] Electrochemical CO_2 reduction (eCO_2R) to produce value-added chemicals is one of the most significant CCUS technologies owing to its high potential to achieve net-zero carbon emission through

integration with renewable energy sources. Although eCO_2R has a relatively low level of technological readiness, recent developments have markedly improved its practical feasibility.

Among the various components of the eCO_2R system, a state-of-the-art electrolyser or reactor that directly supplies gaseous CO_2 to the catalyst layer through a gas diffusion electrode (GDE) considerably improves the scale and selectivity of the reaction (Fig. 1a), leading to record-breaking current densities ranging from hundreds of mA cm^{-2} to several A cm^{-2}.[5,6] In addition, the conventional eCO_2R achieves a high Faradaic efficiency (FE) of more than 90% and 80% in the case of C_1 (*i.e.* CO and formate)[7,8] and C_{2+} (*i.e.* ethylene, ethanol acetate, *n*-propanol, *etc.*)[9,10] compounds, respectively. Nevertheless, techno-economics analysis (TEA) indicates that the economic viability of the eCO_2R system is limited considering the current levels of technology and the market price of the target chemicals.[11,12] The energy-intensive upstream utilisation of CO_2 as a reactant gas is one of the factors undermining the technological competitiveness of eCO_2R.[13] Expensive, energy-intensive processes such as CO_2 absorption, desorption, and CO_2 compression are required to supply high-purity CO_2 from flue gas or even direct air capture (DAC). For instance, CO_2 capture using a commercially available CO_2 absorbent, such as monoethanolamine, requires up to 4.3 GJ $t_{CO_2}^{-1}$ for amine regeneration.[14,15] This drawback compromises the environmental sustainability of the technology. To implement a profitable and environmentally

[a]Clean Energy Research Center, Korea Institute of Science and Technology, Seoul 02792, Republic of Korea. E-mail: dahye0803@kist.re.kr

[b]Department of Chemistry, Kookmin University, Seoul 02707, Republic of Korea

[c]Department of Chemistry, Seoul National University, Seoul 08826, Republic of Korea. E-mail: yjhwang1@snu.ac.kr

[d]Division of Energy and Environmental Technology, KIST School, Korea University of Science and Technology (UST), Seoul 02792, Republic of Korea

[e]Graduate School of Energy and Environment (Green School), Korea University, Seoul 02841, Republic of Korea

[f]Department of Chemical and Biomolecular Engineering, Yonsei-KIST Convergence Research Institute, Yonsei University, Seoul 03722, Republic of Korea

[g]Center for Nanoparticle Research, Institute for Basic Science (IBS), Seoul 08826, Republic of Korea

[h]KHU-KIST Department of Converging Science and Technology, Kyung Hee University, Seoul 02477, Republic of Korea

† These authors contributed equally to this work.

This journal is © The Royal Society of Chemistry 2024

J. Mater. Chem. A, 2024, **12**, 10597–10613 | **10597**

sustainable eCO_2R system, an advanced system linking low-concentration CO_2 capture and conversion is critical.

The direct electrochemical conversion of captured CO_2 (capt-eCO_2R) has recently been recognised as a state-of-the-art eCO_2R system that simplifies the system configuration (Fig. 1b). Rather than relying on gaseous CO_2 as a reactant, this system directly utilises captured CO_2 in CO_2 absorbent and thus integrates the CO_2 capture and electrochemical conversion processes. Unreacted CO_2 gas is absorbed in the reaction media (*i.e.*, CO_2 absorbent), allowing concentrated gas products to be obtained from the capt-eCO_2R. In contrast, the conventional gas-fed eCO_2R system (gas-eCO_2R) necessitates an additional process to separate the gas products from the unreacted CO_2 gas. Thus, in principle, systems that directly convert captured CO_2 conversion do not require energy-intensive processes such as CO_2 conditioning (CO_2 desorption and compression) and product separation, which are essential in gas-eCO_2R (Fig. 1c).[16] Based on these intrinsic advantages, a few studies have compared the life cycle analysis (LCA) and TEA of capt-eCO_2R systems with those of gas-eCO_2R systems. Langie *et al.* compared the LCA and TEA of the direct electrochemical conversion of triethylamine (TREA) captured CO_2 with those of several syngas production CCU systems such as the reverse water gas shift reaction and conventional gas-eCO_2R.[17] The capt-eCO_2R system using TREA recorded the most favourable operating expenditure (OPEX) and lowest break-even syngas price. Moreover, evaluation of the global warming potential (GWP) through global sensitivity analysis showed that the capt-eCO_2R system using TREA can achieve near net-zero CO_2 emissions, making the capt-eCO_2R system industrially feasible, environmentally sustainable, and economically viable. Despite these advantages, the performance of capt-eCO_2R is rather low;

however, LCA/TEA analyses suggest that improving the current density at lower overpotentials may make the system more compelling. A similar direction of development was proposed by Gao *et al.*, who found that lower capital expenses could be achieved with capt-eCO_2R, but a carbon-negative system still requires high current densities of over 0.15 A cm^{-2}.[18] Therefore, to implement a profitable and environmentally sustainable system, improving technological maturity through technical development and a greater theoretical understanding of the capt-eCO_2R is urgently required.

In this study, we investigated various capt-eCO_2R systems that employ different types of electrolysers and absorbents. The solvent in such systems acts as both a CO_2 absorbent and an electrolyte, thus determining the form of the captured CO_2 (*e.g.*, carbamate, bicarbonate/carbonate, *etc.*). Furthermore, because the CO_2 reactant is captured in a liquid solvent, system components such as electrodes, membranes, electrolytes, electrolysers, and other parameters should differ from those of the conventional gas-eCO_2R system. Therefore, this review has a particular focus on the role of the system elements, the reaction mechanism of the capt-eCO_2R, and strategies to improve performance based on the form of the captured CO_2 and the type of solvent. A perspective on an advanced future capt-eCO_2R system with industrial applications is also presented.

2. Direct conversion of captured CO_2

The capt-eCO_2R system achieves the electrochemical conversion of captured CO_2 in a liquid electrolyte without additional feeding of gaseous CO_2 (Fig. 1b). In this system, carbamates or bicarbonate/carbonates, the dominant forms of captured CO_2
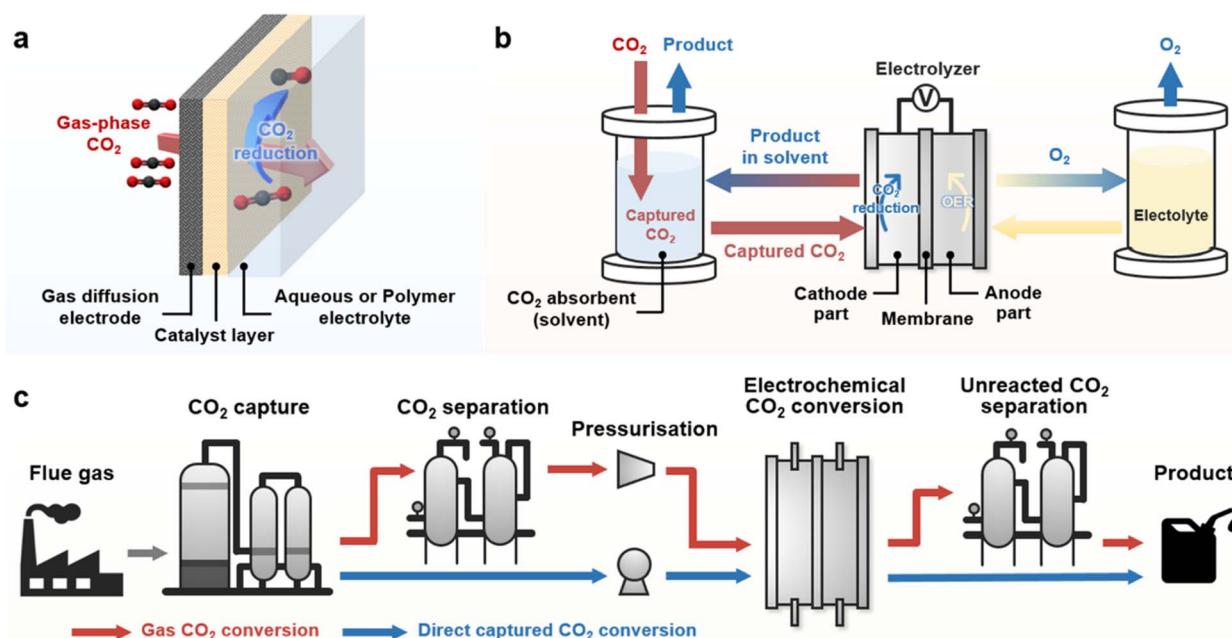
Fig. 1 (a) Schematic of the GDE electrolyser for eCO_2R. (b) System for capt-eCO_2R. (c) Comparison of the systematic pathway of conventional gas-eCO_2 (red line) and capt-eCO_2R (blue line).

10598 | *J. Mater. Chem. A*, 2024, 12, 10597–10613

This journal is © The Royal Society of Chemistry 2024

Table 1 CO_2 capture agents and its capture ability and capture form of CO_2

CO_2 capture agent		Capture ability	Concentration	Capture condition	Capture form	Reference
Metal hydroxide	KOH	~0.745 mol_{CO_2} mol_{KOH}^{-1}	0.412 mol L^{-1}	35 °C, 4 bar[a]	Bicarbonate	19
Primary amine	Monoethanolamine	0.58 mol_{CO_2} mol_{amine}^{-1}	30 wt%	40 °C, 1 bar[b]	Carbamate	20
Secondary amine	Diethanolamine	0.53 mol_{CO_2} mol_{amine}^{-1}	30 wt%	40 °C, 1 bar[b]	Carbamate	20
Tertiary amine	Triethanolamine	0.39 mol_{CO_2} mol_{amine}^{-1}	30 wt%	40 °C, 1 bar[b]	Bicarbonate	20
	Triethylamine	~0.193 mol_{CO_2} mol_{amine}^{-1}	3 M	R. T. ambient[c]		17

[a] The capture ability is evaluated by feeding 99% CO_2. [b] The capture ability is evaluated by feeding 15% CO_2 and 85% N_2 concentration. [c] The capture ability is evaluated by feeding 5% CO_2 concentration in flue gas.

in the aqueous absorbent, are utilised directly as reactants. The formation of carbamate or bicarbonate is determined by the type of absorbent used. The capture abilities and forms of major CO_2 absorbents are outlined in Table 1. Primary and secondary amines capture one CO_2 molecule per two amine molecules, primarily as a carbamate. Theoretically, tertiary amines can capture one CO_2 molecule per one amine molecule, but the reported low CO_2 capture ability appears to be due to a slow CO_2 absorption rate. Potassium hydroxide (KOH) captures one CO_2 molecule per one molecule, but salt formation hinders the recording of the theoretical CO_2 capture ability. Considering that the optimal CO_2 absorbent concentrations for primary/ secondary amines and tertiary/KOH are 30 wt% and 3 M, respectively, the concentrations of carbamate and bicarbonate/ carbonate would be similar regardless of the types of CO_2 absorbents used. Therefore, in this review, we categorised the previous studies based on the forms of the captured CO_2 (Fig. 2). As carbamate and (bi)carbonate electrolytes have different reaction mechanisms, their utilisation requires different strategies and approaches.

2.1 CO_2 captured in carbamate form

Many primary and secondary amines, such as monoethanolamine, diethanolamine (DEA), 2-amino-2-methyl-1-propanol (AMP), and their mixtures, are commercially available CO_2 absorbent, primarily capturing CO_2 as carbamates ($RNHCOO^-$). Therefore, CO_2 captured by these types of amines can be easily integrated into established industrial processes; however, the

utilisation of carbamate can prove challenging owing to the very strong C–N bond, which necessitates the use of an energy-intensive amine regeneration process.[21,22] Furthermore, the negatively charged moiety of the carbamate results in electrostatic repulsion between the cathode and carbamate. Several approaches have been developed to overcome the limitations imposed by the intrinsic properties of carbamate.[2,23,24]

2.1.1 Monoethanolamine media. Monoethanolamine is the most common adsorbent used in the direct conversion of captured CO_2. Chen et al. first achieved capt-eCO_2R in a monoethanolamine medium by experimentally screening several metal candidates, including In, Sn, Bi, Pb, Pd, Ag, Cu, and Zn to identify high-performing catalysts in 30% (w/w) monoethanolamine solution.[25] In this experiment, the monoethanolamine solution was saturated with CO_2 for 30 min before the experiment, and capt-eCO_2R was conducted in a gas-tight H-type cell under an Ar atmosphere (Fig. 3a). The main products of these catalysts primarily yielded the same products as conventional gas-eCO_2R, i.e., CO and formic acid; however, the hydrogen evolution reaction (HER), which competes with the eCO_2R, occurred significantly under these operating conditions, thereby reducing the efficiency of the system. Several classes of organic surfactants were added to the monoethanolamine solution to modulate the water access near the electrode and reduce the HER activity, including the cationic cetyl-trimethylammonium bromide (CTAB), anionic sodium dodecyl sulfate (SDS), and the non-ionic Triton X-100 (Fig. 3b and c). CTAB outperformed the other surfactants in increasing the
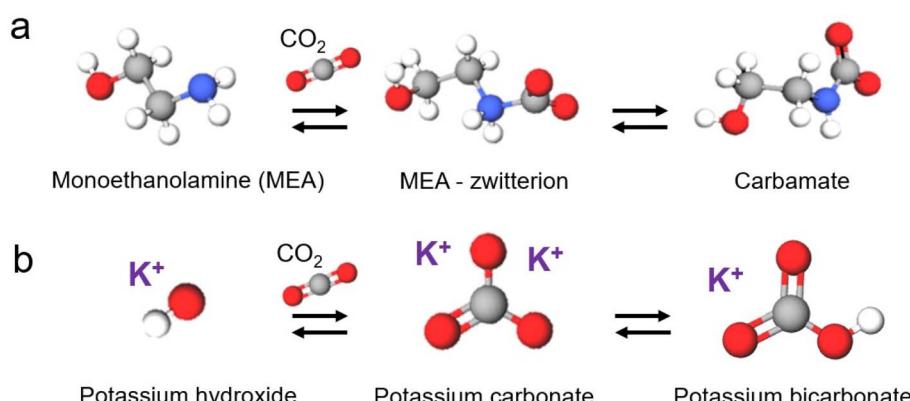
Fig. 2 Reaction mechanism of the direct conversion of CO_2 into (a) carbamate and (b) bicarbonate.

This journal is © The Royal Society of Chemistry 2024

J. Mater. Chem. A, 2024, **12**, 10597–10613 | **10599**
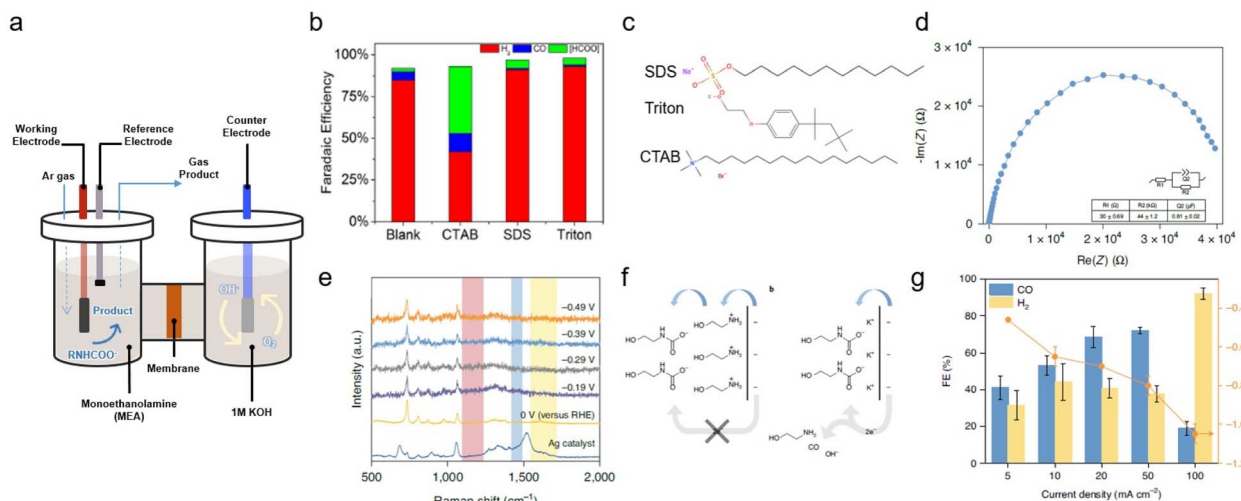
Fig. 3 (a) Schematic of an H-type cell. (b) FE of products obtained with a smooth indium plate at a potential of -0.8 V vs. RHE in monoethanolamine containing 0.1% (w/w) of various surfactants. (c) Structures of the examined surfactants. Copyright 2017,[25] Wiley. (d) EIS of the monoethanolamine/KCl electrolyte collected at open circuit potential, approximately -0.145 V vs. Ag/AgCl. Inset: the equivalent circuit and fit values of each component. R_1 and R_2 are the series and charge transfer resistances, respectively; Q_2 is the constant phase element. The error of each component denotes the standard deviation of three independent measurements. (e) In situ surface-enhanced Raman spectra of the monoethanolamine/KCl electrolyte. (f) Proposed interfacial structure near the electrode surface. (g) Product distribution of monoethanolamine-CO_2 conversion to H_2 and CO at different applied current densities, ranging from 5 mA cm^{-2} to 100 mA cm^{-2} in a flow cell system. Copyright 2020,[24] Springer Nature.

capt-eCO$_2$R selectivity over the HER (Table 2). For instance, the In electrode achieved enhanced the FE of CO from 4.8 to 17% and that of formate from 2.4 to 45.4%.

A similar monoethanolamine utilisation system was developed by Lee et al.; however, this system also exhibited low capt-eCO$_2$R performance.[24] In CO$_2$-saturated monoethanolamine solution, a Ag catalyst showed a CO FE of just 5% in the potential range from -0.46 to -0.78 V. Electrochemical impedance spectroscopy (EIS) and in situ Raman analysis of capt-eCO$_2$R in monoethanolamine solution showed the formation of an electrochemical double layer (EDL) composed of ethanol–ammonium ions and carbamate. Due to the cationic ethanol–ammonium ion forming an inner Helmholtz layer owing to the negatively biased electrode surface, electron transfer must first pass through the ethanol–ammonium ion before reaching carbamate, which consequently inhibits the facile conversion of carbamate (Fig. 3f). Various alkali cations, such as Li$^+$, Na$^+$, K$^+$, Rb$^+$, and Cs$^+$, were added to the electrolyte to systematically tune the EDL. Among the various alkali cations, K$^+$ significantly improved the capt-eCO$_2$R performance,

by facilitating the adjustment of EDL, as evidenced by data from EIS and in situ Raman analysis (Fig. 3d and e). The addition of Li$^+$ and Na$^+$ resulted in the production of less CO than the pure monoethanolamine solution. This trend correlates with the ionic radius of the cations owing to differences in water solvation. Increasing the reaction temperature to facilitate cleavage of the C–N bond can also improve the performance of the system. The current density at 60 °C was 15 times higher than that at room temperature. By adjusting the EDL with a high concentration of alkali salt, 2 M KCl, and circulating the catholyte at 60 °C in the flow cell, CO production remarkably increased to 72% at 50 mA cm^{-2} and -0.8 V versus reversible hydrogen electrode (RHE) by directly utilising monoethanolamine captured CO$_2$ (Fig. 3g).

To understand the capt-eCO$_2$R system, its catalytic activity was investigated in various absorbent media. Atomically dispersed nickel-doped carbon (Ni–N/C), a promising capt-eCO$_2$R catalyst, was applied in CO$_2$-captured 5 M monoethanolamine solutions (Fig. 4a and b).[26] The Ni–N/C catalyst has demonstrated high CO production selectivity comparable to

Table 2 FE of various products during capt-eCO$_2$R on various metal electrodes in CO$_2$-saturated 30% (w/w) monoethanolamine solution with 0.1% (w/w) CTAB[25]

F.E. (%)	In			Sn			Bi			Pb			Pd			Ag			Cu			Zn		
$-V_{RHE}$	0.8	1.1	1.3	0.8	1.1	1.3	0.8	1.1	1.3	0.8	1.1	1.3	0.1	0.5	0.8	0.8	1.1	1.3	0.8	1.1	1.3	0.8	1.1	1.3
H$_2$	41.9	42.0	44.3	68.6	78.5	93.4	69.5	87.1	93.4	79.6	79.2	85.1	91.6	87.3	96.0	62.8	84.7	89.5	79.7	98.1	91.0	103.0	91.4	102.0
CO	17.0	10.7	11.2	9.0	3.6	2.6	7.0	4.9	2.6	1.9	3.0	3.5	—	—	—	33.4	15.9	9.2	1.7	—	—	3.7	2.9	0.5
HCOOH	45.4	39.4	36.5	19.0	16.4	2.0	24.3	7.1	3.9	8.5	8.7	6.1	4.0	4.1	0.1	2.0	2.8	1.7	19.1	0.5	0.1	5.4	2.0	2.0
Total	104.3	92.1	92.0	96.6	98.5	98.0	100.8	99.1	99.9	90.0	90.9	94.7	95.6	91.4	96.1	100.8	103.4	100.4	100.5	98.6	91.1	112.1	96.3	104.5

10600 | J. Mater. Chem. A, 2024, 12, 10597–10613

This journal is © The Royal Society of Chemistry 2024
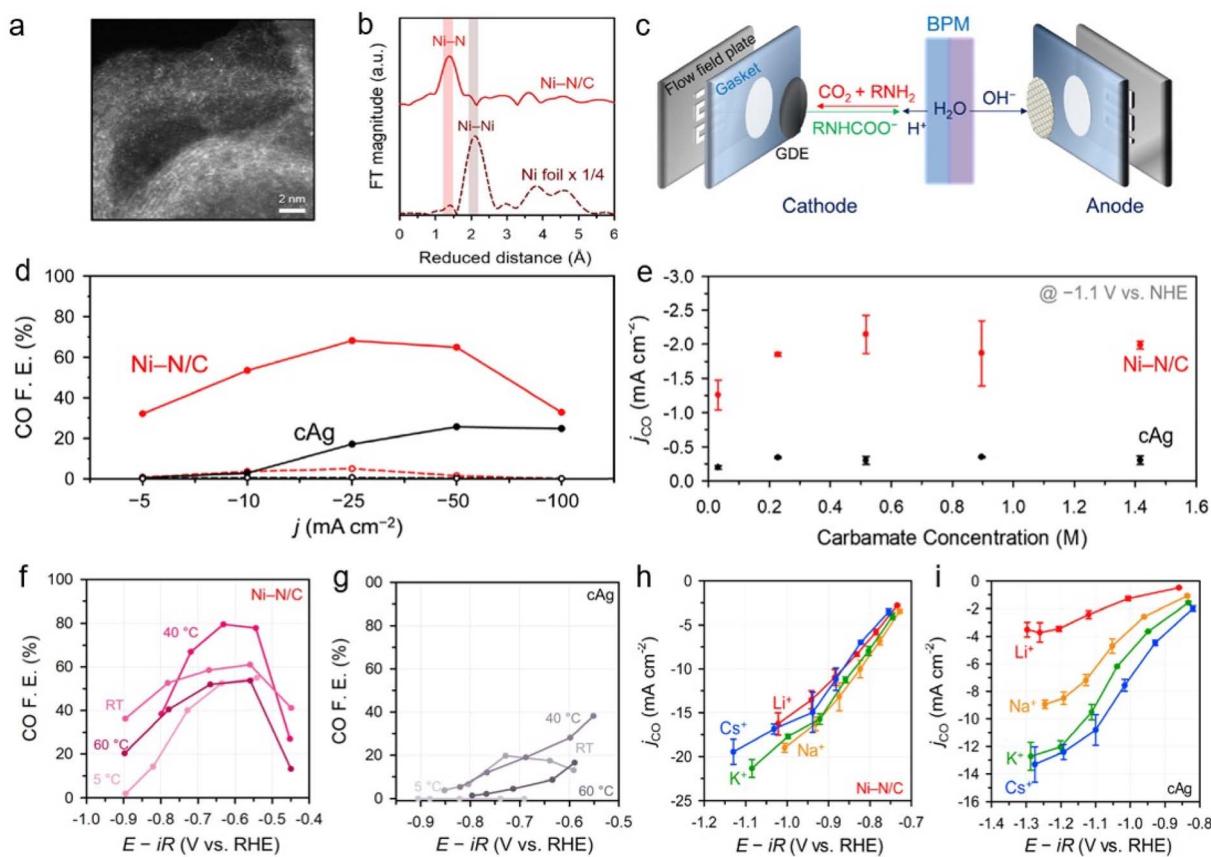
Fig. 4 Physical characterisation of Ni−N/C (a) high-angle annular dark-field scanning transmission electron microscopy image. (b) Extended X-ray absorption fine structure spectra of Ni−N/C and Ni-foil. (c) Schematic of capt-eCO$_2$R in MEA cell with BPM, anode and cathode. (d) Ni−N/C and cAg performance in membrane electrode assembly using 5 M monoethanolamine. (e) j_{CO} of Ni−N/C and cAg with respect to carbamate concentration. CO FE of (f) Ni−N/C and cAg (g) at various temperatures. Cation effect and sensitivity of Ni−N/C (h) and cAg (i) by occupying conventional gas-eCO$_2$R. Copyright 2020,[26] Royal Society of Chemistry.

that of a Ag catalyst, while the atomically dispersed active sites efficiently suppress the HER. Using Ni−N/C in an H-type electrolyser using CO$_2$-captured 5 M monoethanolamine solutions, they achieved a CO partial current density three times higher than that obtained with a commercial Ag electrode (cAg). Furthermore, the introduction of a zero-gap membrane electrode assembly (MEA) equipped with a bipolar membrane (BPM) (Fig. 4c) improved the system efficiency, with Ni−N/C resulting in a 64.9% CO FE at −50 mA cm^{-2}, 2.5 times higher than that obtained using the cAg (Fig. 4d). To understand the catalytic performance of the Ni−N/C catalyst, the reaction mechanisms were investigated by adjusting the carbamate concentration (from 1 M to 5 M monoethanolamine) (Fig. 4e). Interestingly, the reaction rate was unaffected by the carbamate concentration, indicating a zeroth-order dependence on the carbamate concentration in this range. This implied that the CO$_2$ released from the carbamate, rather than the carbamate itself, is the main reactant in the capt-eCO$_2$R. Temperatures higher than 60 °C typically favoured H$_2$ generation and thus reduced CO selectivity (Fig. 4f and g). The similarity between the capt-eCO$_2$R pathway and the conventional gas-eCO$_2$R pathway leads to the high performance of the Ni−N/C catalyst in the CO$_2$-

capturing amine-based solvent, which is attributed to its outstanding intrinsic activity. The performances of Ni−N/C and cAg in the capt-eCO$_2$R were further investigated in different CO$_2$ capturing media, such as 1 M 3-amino-1-propanol, 2-(methylamino)ethanol, AMP, DEA, and KHCO$_3$, in order to investigate the effect of bulky cations. Considering that alkali metal cations with a smaller effective size have a higher surface density and thus stabilise the CO$_2$-intermediate, the Ni−N/C exhibited remarkable CO FE performance irrespective of the type of electrolyte. Additionally, the CO FE of cAg decreases significantly as the cation size increases. The weak cation sensitivity of Ni−N/C was further demonstrated in M$_2$CO$_3$ electrolytes containing various alkali metal cations (M = Li$^+$, Na$^+$, K$^+$, and Cs$^+$) (Fig. 4h and i). This unique feature of Ni−N/C may be derived from its potential for zero charge (PZC), which is higher than that of cAg. The high PZC of Ni−N/C was thought to increase the surface charge density, which in turn reduces the impact of the steric bulk of the cation on surface intermediate stabilisation, thereby showing universal performance. This further highlights the importance of charge density at the EDL in improving the capt-eCO$_2$R, in addition to its inherent catalytic activity.

This journal is © The Royal Society of Chemistry 2024

J. Mater. Chem. A, 2024, **12**, 10597–10613 | **10601**
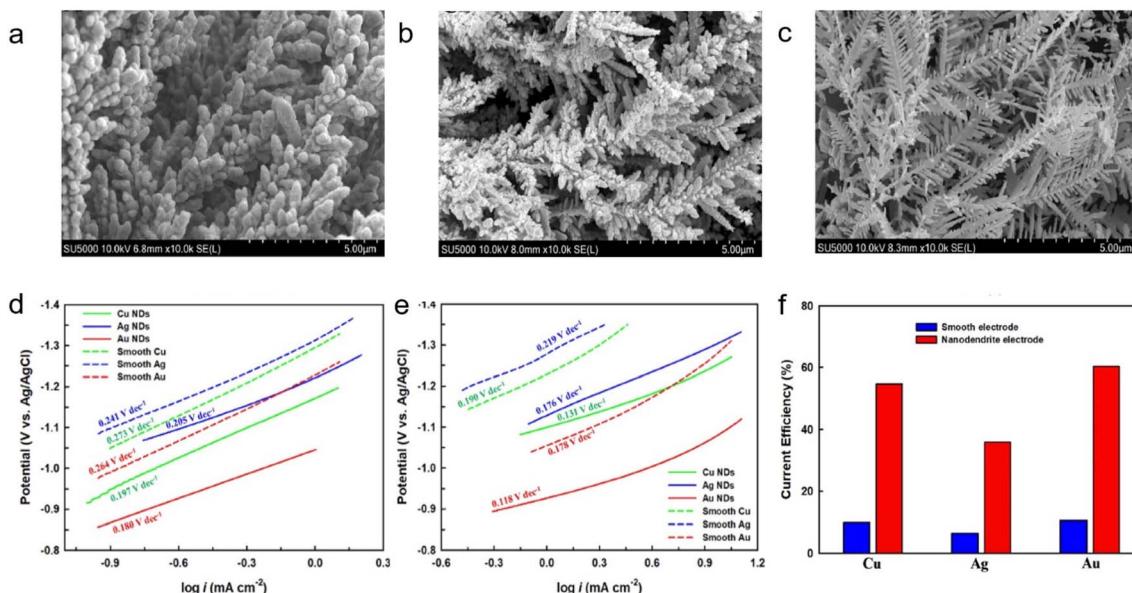
Fig. 5 SEM images of as prepared (a) Cu, (b) Ag, and (c) Au nanodendrites. Tafel slope of various electrodes in CO_2-saturated solutions of (d) 0.1 M $NaHCO_3$ and (e) 0.05 mol fraction ethanolamine solution. (f) Current efficiency of smooth and nanodendritic electrodes in CO_2-saturated 0.05 mol fraction ethanolamine solution at -1.0 V (vs. Ag/AgCl). Copyright 2021,[27] Wiley.

Modification of the catalyst morphology is an effective strategy for improving performance and has been applied to the capt-eCO_2R system. Hossain et al. prepared Cu, Ag, and Au nanodendrites and conducted the capt-eCO_2R in CO_2-captured 0.05 M ethanolamine solutions (Fig. 5a–c).[27] The nanodendrites exhibited a high electrochemically active surface area with a large double-layer capacitance, and consequently showed a higher eCO_2R current density than a smooth surface. The Au nanodendrites outperformed the other electrodes, showing the highest current efficiency and lowest onset potential. These properties may arise from the synergistic effect between the dendritic structure and the intrinsic activity of Au, which is a well-known catalyst for CO production. The as-synthesised Au nanodendrites showed the most efficient eCO_2R with a high current density in the linear sweeping voltammetry studies and recorded the lowest Tafel slope (Fig. 5d and e). A comparison of the eCO_2R performance of nanodendrites in CO_2-saturated $NaHCO_3$ and CO_2-saturated ethanolamine demonstrated that ethanolamine is a promising absorbent for the capt-eCO_2R system. Ethanolamine plays an important role in achieving high current density and catalytic activity because the protonated NH_3^+ group of ethanolamine increases CO_2 solubility.[28,29] Furthermore, as-synthesised Au nanodendrites exhibited a significant performance in capt-eCO_2R in ethanolamine, demonstrating its potential as a catalyst in this system (Fig. 5f).

Recent studies have identified the active species in the reduction of CO_2 in monoethanolamine-containing aqueous electrolytes.[30] The carbamate moiety is not the only active site in aqueous monoethanolamine, and bicarbonate formation occurred as the partial pressure of CO_2 increased, as detected by ^{13}C NMR. This bicarbonate was formed via carbamate hydrolysis and was confirmed by the reduction in pH as the bicarbonate concentration and CO_2 pressure increased. Though the reduction of CO_2 to CO in monoethanolamine is limited by the adsorption of dissolved CO_2, the addition of proton-donating ammonium cations influences the HER. Further study is required to achieve a better understanding of the active state of monoethanolamine during CO_2 reduction.

2.1.2 Other types of solvents media. Although monoethanolamine is the most common industrial CO_2 absorbent, capt-eCO_2R systems can employ other types of solvents. Bhattacharya et al. studied the ability of a series of primary, secondary, and tertiary amines to utilise carbamates/carbamic acid as a CO_2 source.[31] The primary amines included tetramethylguanidine (TMG) and aniline, the secondary amines were morpholine, DEA, and dimethylamine (DMA), and the tertiary amines were TREA and triethanolamine (TEOA) (Fig. 6a). The tertiary amine may absorb CO_2 as bicarbonate, as discussed in detail in Section 2.2.2. Employing glassy carbon as the working electrode, the only product produced was formate; CO and H_2 were not detected in this system. The contribution of amines was examined by cyclic voltammetry (CV) in the presence and absence of CO_2. TMG traps more CO_2 than the other amines and therefore drives the equilibrium towards carbamate. TMG reacts as a Brønsted base towards CO_2 owing to its steric bulk, while the other amines are Lewis bases. Upon the addition of CO_2, the Infrared (IR) spectra showed the presence of carbamate species. No carbonate or bicarbonate vibrations were detected in the IR spectra when water was added, indicating that no other species were formed. In this study, TMG was added to stabilise the carbamates of the other selected amines. In the absence of TMG, no significant peaks related to any amines were observed. In the presence of TMG, all the CV data shifted owing to the formation of carbamate. Among the tertiary

10602 | J. Mater. Chem. A, 2024, **12**, 10597–10613

This journal is © The Royal Society of Chemistry 2024
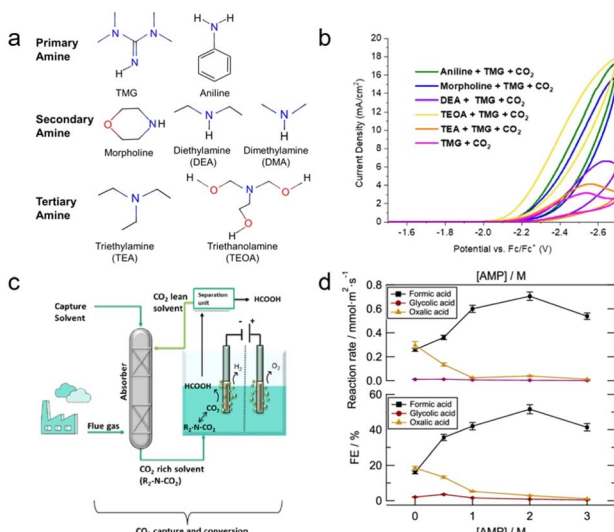
Fig. 6 (a) Primary, secondary, and tertiary amines tested in this experiment. (b) CV responses of various amines in the presence of CO_2 and 0.1 M TMG at a scan rate of 0.1 V s^{-1}, scanning negative. Copyright 2020,[31] The Electrochemical Society. (c) The proposed CO_2 capture and conversion system. (d) AMP concentration effect of reaction rate and FE of formate, glycolate, and oxalate during electrolysis at -2.5 V *vs.* Ag/AgCl at 75 °C. Copyright 2021,[32] American Chemical Society.

amines, only TEOA shifted the onset potential to a less negative value in the presence of TMG. Aniline, TEOA, and morpholine underwent complexation with CO_2, resulting in higher current densities in CV tests (Fig. 6b). This suggests that these amines have a greater ability to bind redox-active CO_2 in solution. Interestingly, the bicarbonate content increased in the presence of secondary amines and aniline through an anodic shift of the onset potentials when water was added, while in the carbamate content decreased. These amines resulted in a reduction in potential upon the addition of water to the saturated CO_2 solution, indicating that proton or bicarbonate reduction occurs due to the addition of water. The CV data of the secondary amines and aniline exhibited an anodic shift upon the addition of water, except for TMG, indicating the conversion of carbamate species to bicarbonate. The addition of water had a negligible effect on the CV of TREA because no carbamate species were present.

Pérez-Gallent *et al.* developed an integrated system for CO_2 capture and conversion by combining chemical and physical absorption solvents as electrolytes and increasing the temperature of the system in a mixed solution of AMP and propylene carbonate (PC).[32] The system is functioned by combining these two solvents, where AMP is CO_2 capturing media and PC is the physical solvent. This method involves heating an electrochemical reactor to liberate the captured CO_2 (Fig. 6c). The concentration of AMP affected the reduction of CO_2 at an optimal concentration of 2 M. Further increasing the concentration of AMP to 3 M results in a highly viscous solution that limits the conductivity and mass transfer properties of the solvent (Fig. 6d). Increasing the temperature also affects the performance of the system,[24,26] which will be discussed in detail

in Section 3.3. A Pb catalyst produced formic acid with a FE of up to 45% and a reaction rate of 0.56 mmol m^{-2} s^{-1}. Recent research has indicated that AMP predominantly captures CO_2 in the carbamate form, which undergoes hydrolysis in an aqueous solution to form bicarbonate.[33,34] This phenomenon enhances the efficacy of AMP relative to other primary amines. Bicarbonate conversion is further discussed in Section 2.2.

2.2 (Bi)carbonate conversion

Metal hydroxides such as NaOH and KOH chemically absorb CO_2 to form bicarbonates or carbonates depending on the pH of the solution. Such absorbents offer several advantages over amine absorbents, including lower volatility and absence of odour; however, their industrial application is limited by the drawbacks of salt formation during CO_2 conditioning, high regeneration energy, and corrosivity arising from their high alkalinity.[35-43] Despite these drawbacks, metal hydroxides are currently suitable CO_2 absorbents for DAC systems, owing to their high selective absorption capacity in low-concentration CO_2 environments. Moreover, the application of metal hydroxides to the capt-eCO_2R system can address the high regeneration energy issue because the high-temperature (>700 °C)[44] calcination process to release captured CO_2 is replaced by electrochemical conversion of bicarbonate/carbonate. Therefore, capt-eCO_2R systems using metal hydroxides are promising systems for achieving net-zero CCUS and carbon-negative direct air capture and utilisation (DACU).

Tertiary amines absorbents chemically absorb CO_2 in the form of bicarbonate. Unlike primary and secondary amines, tertiary amines do not directly bond with CO_2 but act as base catalysts in the CO_2 capture process (Fig. 7). Compared to primary and secondary amines, the C–H bonds of tertiary amines give an energetical advantage over the C–N bonds of primary and secondary amines in the desorption process. Additionally, tertiary amines generally have a higher capacity because one tertiary amine molecule captures one CO_2 molecule, whereas two molecules of primary and secondary amines are required to capture one CO_2 molecule as mentioned in Section 2. The performance of tertiary amine-based systems is expected to depend on the amine type, given that metal hydroxides provide the alkali cations required for electrochemical conversion reactions.

2.2.1 Alkaline media. The direct electrochemical conversion of $KHCO_3$ is known to exhibit low selectivity and current density in a conventional H-type cell system.[45,46] Li *et al.* introduced a new reactor configuration to present a new reaction pathway for the direct utilisation of bicarbonate (Fig. 8a).[47] This method employs a MEA electrolyser with a BPM to separate water into H^+ and OH^- using an induced electric field. The cation- and anion-exchange layers of the BPM contacted the cathode and anode, respectively, to deliver H^+ to the cathode under a reverse bias (Fig. 8b). This creates an acidic environment at the cathode surface, and consequently, the bicarbonate in the catholyte circulating towards the cathode is instantly converted to CO_2 because of the pH equilibrium reaction. The CO_2 generated in this manner is called *in situ* CO_2. The *in situ*

This journal is © The Royal Society of Chemistry 2024

J. Mater. Chem. A, 2024, **12**, 10597–10613 | **10603**
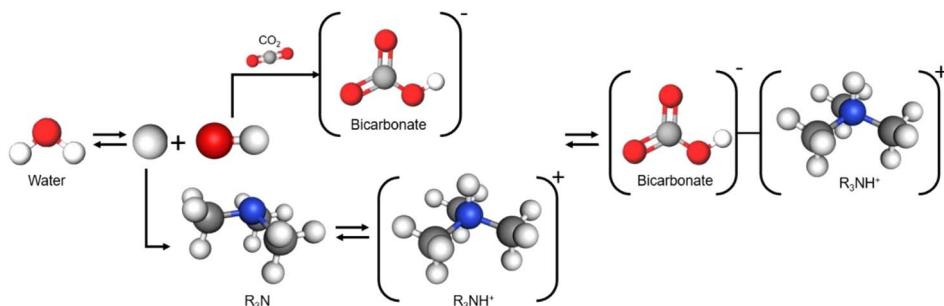
Fig. 7 Representation of the process of CO_2 capture by tertiary amines.

CO_2 receives electrons from the electrode and is reduced to produce CO. The suggested reaction pathway was verified experimentally by replacing the BPM with an anion exchange membrane (AEM) that does not transfer protons in the same cell system. The efficiency of the reactor containing the AEM was significantly lower than that of the reactor containing the BPM, indicating that the reaction occurred *via* the proposed reaction pathway. In this system, the bicarbonate conversion efficiency increased to 81% CO FE at -25 mA cm^{-2} and 37% CO FE at -100 mA cm^{-2} in 3 M KHCO$_3$ (Fig. 8c), thereby overcoming the low selectivity and activity observed in existing systems. This advancement paves the way for further exploration into the direct conversion of bicarbonate. In a follow-up

study, Lees *et al.* analysed the same flow cell configuration using a continuum model.[48] The modeling data presented the concentration distribution of bicarbonate ions, CO_2, pH, and CO_3^{2-} from the cation-exchange layer of BPM to the catalyst layer as a function of the current density and water dissociation performance of BPM (Fig. 8d–g). The model supported a previously proposed mechanism[47] based on simulations and experimental results and also suggests that performance results can be improved by adjusting factors such as the thickness of the catalyst layer and the efficiency of the BPM.

The bicarbonate conversion products were diversified by using different catalyst materials. Similar to conventional gas-eCO$_2$R, the major products are determined by the type of
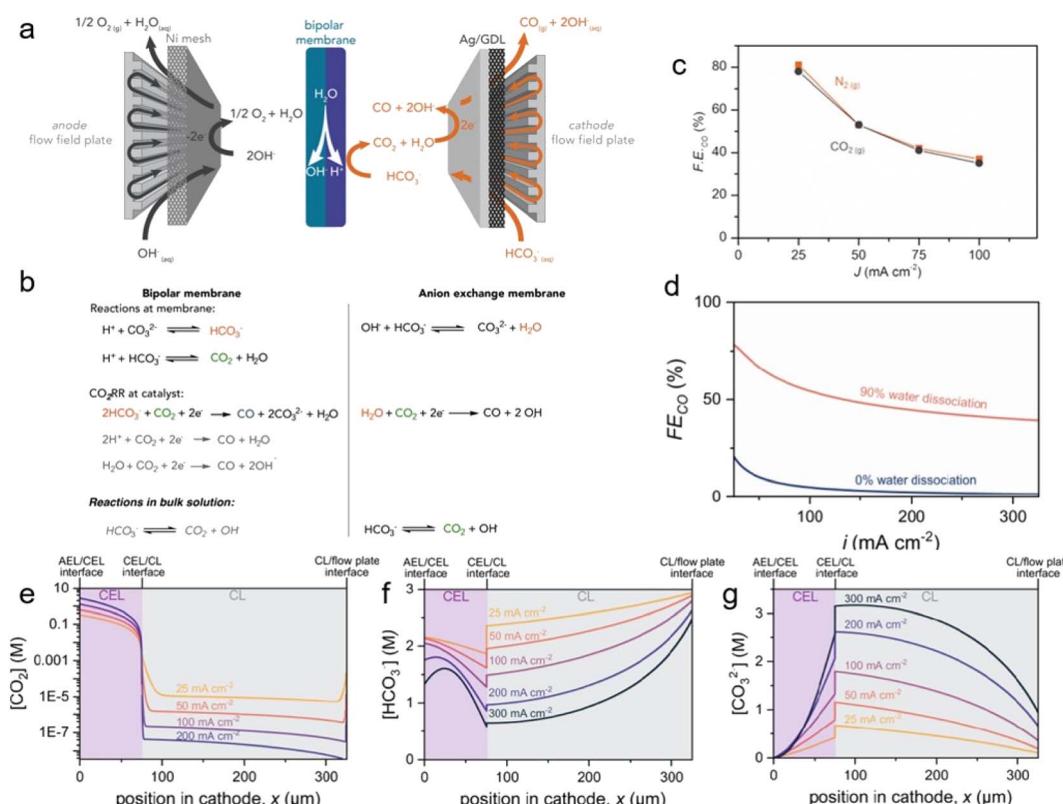
Fig. 8 (a) Schematic of the MEA electrolyser with BPM. (b) The proposed dominant reactions that occur using each membrane. (c) CO FE between 25 and 100 mA cm^{-2} in a 3.0 M KHCO$_3$ solution. Copyright 2019,[47] Elsevier. (d) CO FE as a function of the water dissociation performance of BPM in the bicarbonate electrolyser cathode. Modeling results of (e) CO_2, (f) HCO$_3^-$, (g) CO_3^{2-} concentrations at various current densities. Copyright 2022,[48] American Chemical Society.

10604 | *J. Mater. Chem. A*, 2024, **12**, 10597–10613

This journal is © The Royal Society of Chemistry 2024

catalyst. CO is primarily produced using Ag catalysts. Zhang *et al.* used a cathode consisting of porous Ag foam that showed high activity of 59% CO FE at -100 mA cm^{-2} in 3 M KHCO$_3$ (Fig. 9b).[49] Kim *et al.* reported that Ni–N/C showed significantly higher selectivity (91.0%) than cAg catalyst (28.8%) at -0.65 V$_{RHE}$ in 1 M KHCO$_3$ (Fig. 9c).[26] In addition, Li *et al.* noted that the H$_2$: CO ratio of syngas, the feedstock for the Fischer–Tropsch reaction, varied from 2.5 : 1 to 7 : 1, and they produced a 3 : 1 ratio of syngas from CO$_2$ captured 2 M KOH using a Ag catalyst.[50] In particular, they also showed operational stability of 145 hours in the system. As a study on the production of formate, Bonet Navarro *et al.* used a bulk Sn catalyst to obtain 18% and 47% formate FE in 1.5 M KHCO$_3$ in the case of CO$_2$ pre-saturated and CO$_2$ pre-saturated 1.5 M KHCO$_3$, respectively, at -1.6 V *vs.* Ag/AgCl.[51] In addition, Li *et al.* reported that electrodeposited Bi on carbon paper produced formate with 64% FE at -100 mA cm^{-2} and 27% FE at -400 mA cm^{-2} in 3 M KHCO$_3$ (Fig. 9a).[52] Lees *et al.* also demonstrated that Cu foam produced methane with a partial current density of -120 ± 10 mA cm^{-2} in 34 ± 7% yield from capt-eCO$_2$R in 3 M KHCO$_3$ with 3 mM CTAB.[53] 1D continuum modeling suggests that multi-carbon products are formed if the H$^+$ supply from the membrane is smoother and the catalyst surface becomes more acidic. To study the multi-carbon products, Lee *et al.* composed a bilayer with one layer consisting of a mixture of Ag catalyst, Nafion, and poly(tetrafluoroethylene) (PTFE) and the other comprising a mixture of Cu catalyst and Sustainion.[54] A flow reactor equipped with this bilayer recorded 41.6 ± 0.39% C$_{2+}$ FE at -100 mA cm^{-2} in 3 M KHCO$_3$ (Fig. 9d).

Another study targeting multi-carbon products found that controlling the microenvironment was crucial, in addition to catalyst design. Lee *et al.* investigated instantaneous CO$_2$ detachment by a pH equilibrium reaction of the absorbed CO$_2$ species according to distances between the membrane and the cathode.[55] The use of a 0.5 M H$_2$SO$_4$ anolyte and Nafion as a cation exchange membrane (CEM) with various thicknesses of interposers enabled the construction of well-defined spacing between 135 and 540 μm (Fig. 10a–c). In this configuration, high C$_{2+}$ FE of 38% at a distance of 135 μm and a current density of -300 mA cm^{-2} were obtained in the presence of Cu nanoparticle catalysts (Fig. 10d). Also noteworthy, the CEM lowered the overpotential of the system by facilitating proton transfer to the cathodic side owing to the concentration gradient (Fig. 10e). To enhance C$_{2+}$ production, cobalt phthalocyanines on carbon nanotubes (CoPc-CNTs) was applied to the Cu to produce CO from CO$_2$ with high turnover frequencies, resulting in a higher C$_{2+}$ FE of 47% at -300 mA cm^{-2} (Fig. 10f). These efficient systems highlight the importance of adjusting the mass transport to improve current density.

2.2.2 Tertiary amine media. Process engineering has been applied to combine the capture and conversion of CO$_2$. Diaz *et al.* applied the concept of switchable polarity solvents (SPS) using a tertiary amine, 1-cyclohexylpiperide (CHP), in which the polarity changes upon CO$_2$ absorption, which results in a change in its water solubility.[56] Based on this property, a reversible amine cycle can be established when CHP is applied as a CO$_2$ absorbent in the capt-eCO$_2$R system (Fig. 11a). A CEM (Nafion) applied MEA with a buffer layer between CEM and cathode was prepared, along with a 1.25 M CHP–H$_2$CO$_3$ solution as a catholyte by
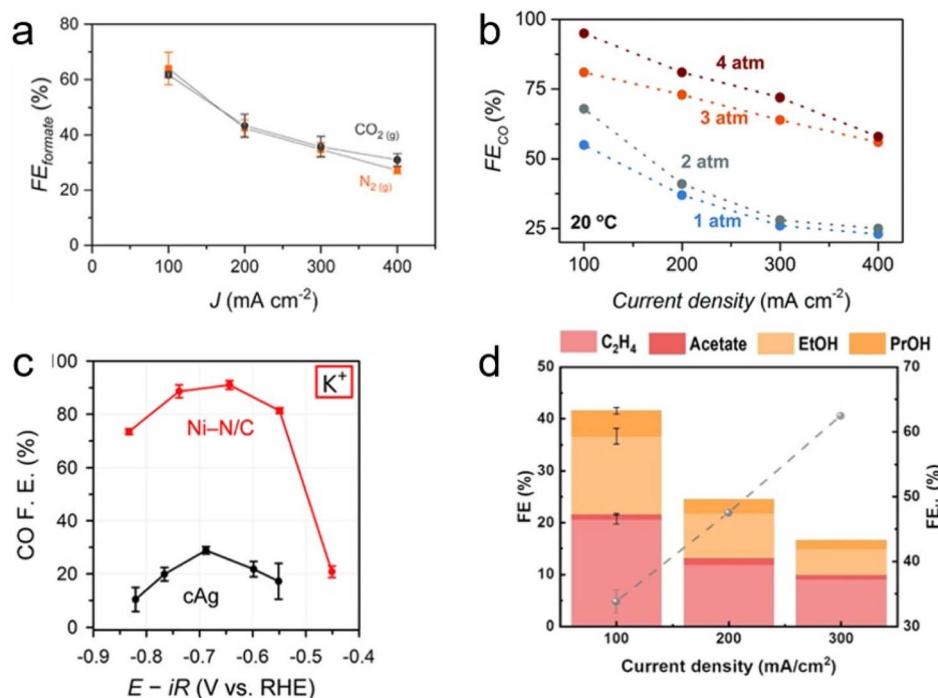
Fig. 9 (a) Formate FE as a function of current density in 3.0 M KHCO$_3$ solution purged with CO$_2$ (g) or N$_2$ (g). Copyright 2020,[52] American Chemical Society. (b) CO FE as a function of pressure at different current densities. Copyright 2022,[49] Royal Society of Chemistry. (c) CO FE of Ni–N/C and cAg in 1 M KHCO$_3$. Copyright 2022,[26] Royal Society of Chemistry. (d) FE of products as a function of current density. Copyright 2022,[54] Wiley.

This journal is © The Royal Society of Chemistry 2024

J. Mater. Chem. A, 2024, 12, 10597–10613 | **10605**
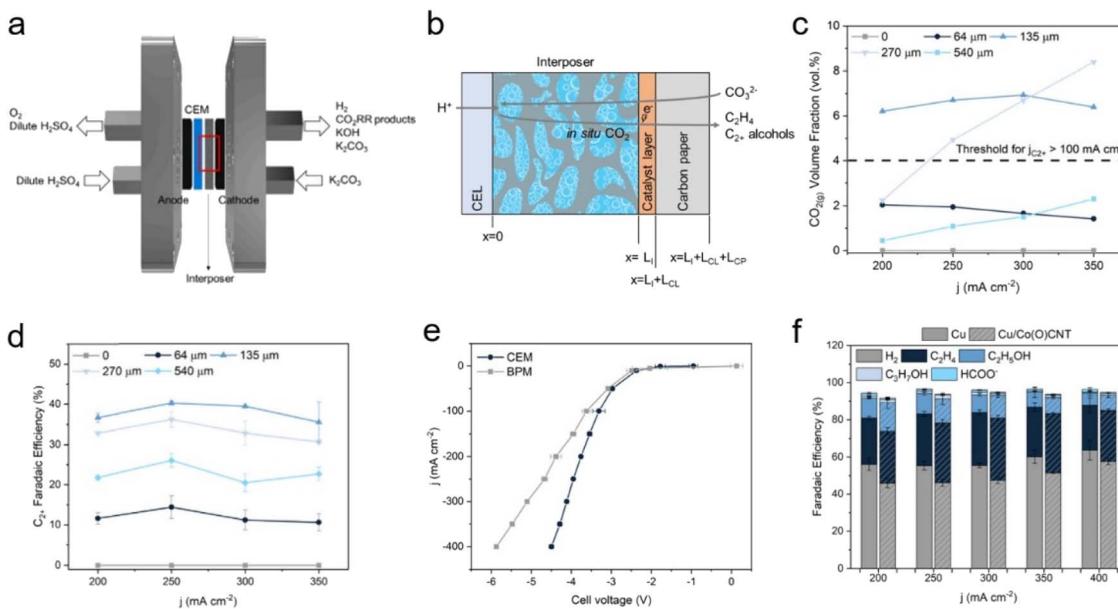
Fig. 10 (a) Schematic of CO_3^{2-}-fed electrolyser. (b) Representation of the cation-exchange layer, interposer, catalyst layer, and carbon paper. (c) CO_2 (g) volume fraction under different spacing conditions and current densities. (d) C_{2+} FE of CO_3^{2-} fed electrolyser with Cu electrocatalyst. (e) Full cell $j-V$ curve with Cu electrocatalyst with a CEM (Nafion) and a BPM in 1.5 M K_2CO_3 solution with 135 μm interposer. (f) Product distribution of Cu electrocatalyst and Cu/CoPc-CNTs catalyst at applied current densities ranging from 200 to 400 mA cm^{-2}. Copyright 2023,[55] Elsevier.

capturing CO_2 in CHP. This concentration (1.25 M) CHP–H_2CO_3 affords the maximum concentration of CO_2 and ionic conductivity. In this configuration, a Ag catalyst showed approximately 30% CO FE at −104 mA cm^{-2} (Fig. 11b). These studies of bicarbonate reduction activity in amine solutions elucidate the behaviour and activity of tertiary amines in the capt-eCO$_2$R.

Langie *et al.* developed a unique bicarbonate conversion system known as a reaction swing absorption (RSA) using TREA as a CO_2 absorbent.[17] The tertiary amine TREA was used in place of a metal hydroxide owing to its high selectivity towards bicarbonate and industrially applicable CO_2 absorption rate. TREA demonstrated a CO_2 absorption rate of 84.5% at a flow rate of 0.8 m^3 h^{-1} with 3% CO_2, and 95.1% at 0.5 m^3 h^{-1} with 3% CO_2, measured in an absorption tower with a height of 3 m (Fig. 12a and b). Various membranes, substrates, and cathode catalysts were evaluated to identify the viable configuration for the utilisation of TREA-captured CO_2. The optimal catalyst for syngas consisted of hydrophilic nano-coral structured Ag with carbon (coral Ag/C), which achieved a CO FE of 68.7% at −20 mA cm^{-2} and 29.2% at

−200 mA cm^{-2} in a BPM equipped MEA electrolyser (Fig. 12c). Remarkably, the CO_2 concentration in the outlet gas is nearly zero, highlighting the effective absorption of TREA and its suitability as a CO_2 absorbent for the capt-eCO$_2$R system. Also, they have reported up to 70 hours of stable performance in TREA capt-eCO$_2$R through the use of optimized catalyst. The feasibility of the RSA system compares favourably with traditional CO_2-to-syngas technologies, such as the reverse water–gas shift reaction and gas-eCO$_2$R, according to TEA and LCA. RSA is in the early stages of development and thus incurs higher capital expenditure (CAPEX) (Fig. 12d); however, it offers the lowest OPEX and break-even prices among the evaluated CCU processes (Fig. 12e). In the optimistic scenario, with potential improvements in CO FE and reduced voltage, the break-even price of RSA could drop to as low as $0.65 per kg of syngas, significantly lowering both the CAPEX and OPEX. The RSA also showed the highest net present value (NPV), indicating a substantial positive increase in profitability (Fig. 12f). LCA showed that RSA had the lowest GWP in all tested scenarios, potentially being as low as 0.27 kg CO_2 eq. kg^{-1} of syngas, moving
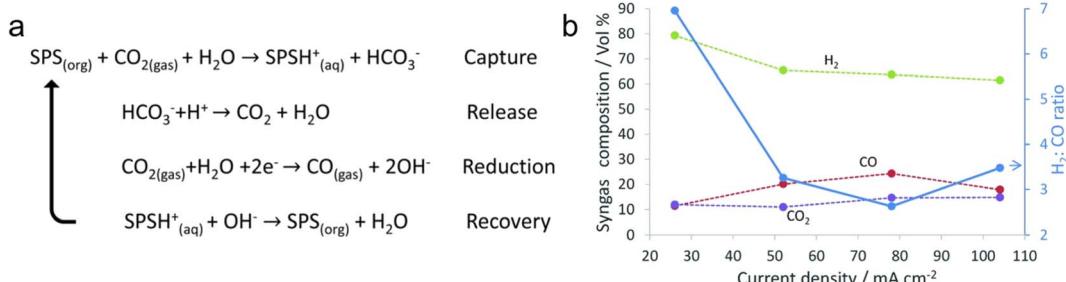

Fig. 11 (a) A proposed amine cycle. (b) $H_2 : CO$ ratio of the syngas obtained at different current densities. Copyright 2018,[56] Royal Society of Chemistry.

10606 | *J. Mater. Chem. A*, 2024, **12**, 10597–10613

This journal is © The Royal Society of Chemistry 2024
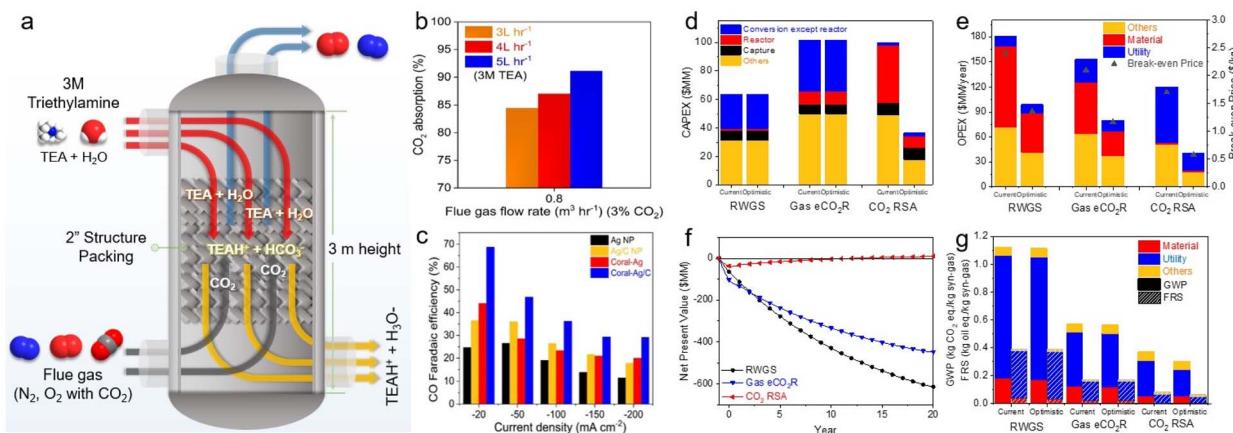
Fig. 12 (a) Schematic of the CO_2 absorption column used in the capture experiments. (b) CO_2 absorption rates at various TREA flow rates at fixed gas flow rate and CO_2 concentration. (c) CO FE of Ag nanoparticle, Ag/C, coral-Ag, and coral Ag/C in 3 M TREA. (d) CAPEX of three processes. (e) OPEX and break-even price of three processes. (f) LCA of the current and optimistic scenarios of three processes. (f) NPV of an optimistic scenario with a selling price of $0.8 per kg syngas. (g) LCA of the current and optimistic scenarios of three processes. Copyright 2022,[17] Springer Nature.

towards net-zero CO_2 emissions (Fig. 12g). These findings highlighted the economic and environmental advantages of bicarbonate systems. Recent achievements in bicarbonate conversion are summarised in Table 3.

To investigate the dependence of the electrochemical activity on the type of tertiary amine, Hosseini *et al.* analysed solutions of monoethanolamine, diethylenetriamine (DETA), diisopropylamine (DIPA), and aminoethylpiperazine (AEP) with and without the addition of bicarbonate using CV.[57] Of these; only DIPA showed a significant catalytic effect on bicarbonate reduction, then the mechanism of carbonate reduction in DIPA was explored electrochemically by scan rate control experiments and EIS analysis.

3 Strategy for improve performance of capt-eCO_2R

Recent studies that aimed to identify the active characteristics of primary amine-based systems have proposed that the release or dissolution of CO_2 may constitute an active component rather than the carbamate itself. Increasing the ratio of free CO_2 to the captured absorbent is important to promote more efficient

utilisation regardless of the absorbent type. Similar strategies have therefore been employed to improve the performance of capt-eCO_2R system, regardless of the type of CO_2 absorbent.

3.1 Control the wettability of electrodes

In the case of an MEA cell or flow cell for the gas-eCO_2R, where reactions occur at a triple-phase boundary, various strategies have been applied to reduce the involvement of water on the solid electrode surface to inhibit the HER and flooding.[60–62] For example, porous carbon paper treated with hydrophobic materials, such as PTFE and microporous layers (MPL), is preferred in the gas-eCO_2R system because it alleviates flooding and enables gaseous CO_2 to access the catalyst layer. In contrast, the capt-eCO_2R requires different mass transport approaches to achieve feasibility because the reactant is delivered in the liquid phase rather than the gas phase. Hydrophobic treatment of the carbon substrate inhibits intimate contact between the liquid reactants and the catalyst layer and may therefore have the opposite effect.

Lees *et al.* compared the performance of Ag catalysts on carbon papers under different PTFE and MPL conditions.[59] Placing the Ag catalyst on carbon paper without PTFE and MPL

Table 3 The capt-eCO_2R performance of reported bicarbonate electrolysers

Catalyst	Catholyte	Product	Faradaic efficiency (%)	Current density (mA cm^{-2})	Temperature	Pressure	Reference
Ag	1.25 M CHP–H_2CO_3	CO	30	−104	25 °C	40 psig	56
Coral Ag/C	3 M TREA	CO	30	−200	R.T.	Ambient	17
Ag foam	1.5 M $CsHCO_3$	CO	80	−100	R.T.	Ambient	58
Ag	3 M $KHCO_3$	CO	82 ± 2	−100	R.T.	Ambient	59
Ag foam	3 M $KHCO_3$	CO	95	−100	R.T.	4 atm	49
Bi	3 M $KHCO_3$	$HCOO^-$	62 ± 1	−100	R.T.	Ambient	52
Cu foam	3 M $KHCO_3$	CH_4	30	−400	R.T.	Ambient	53
Cu/Ag bilayer	3 M $KHCO_3$	C_{2+}	41.6 ± 0.39	−100	R.T.	Ambient	54
Cu/CoPc-CNTs	1.5 M K_2CO_3	C_{2+}	47	−300	R.T.	Ambient	55

This journal is © The Royal Society of Chemistry 2024

*J. Mater. Chem. A*, 2024, **12**, 10597–10613 | **10607**
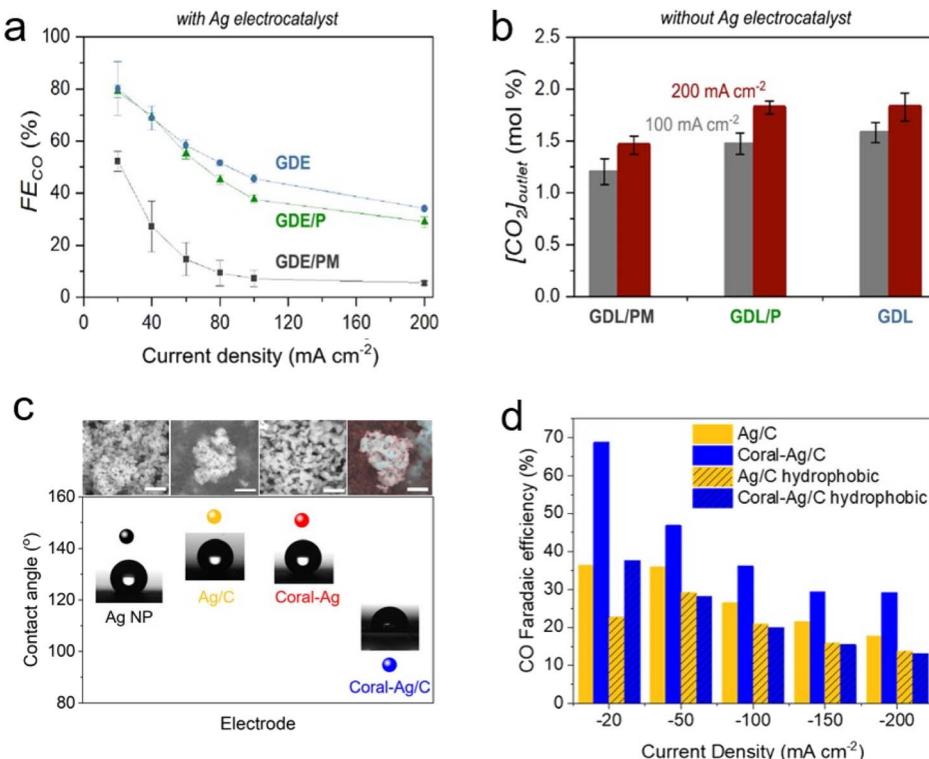
Fig. 13 (a) CO FE of three different electrode conditions; GDE with neither PTFE nor an MPL, GDE/P containing PTFE but with an MPL, and GDE/PM containing both PTFE and an MPL. (b) The concentration of CO_2 in the outlet gas under the three electrode conditions. Copyright 2020,[59] American Chemical Society. (c) SEM images (scale: 500 nm) and contact angles of all Ag electrodes. (d) CO FE of prepared hydrophobic electrodes in the RSA system displayed with those of Ag/C and coral Ag/C. Copyright 2022,[17] Springer Nature.

achieved the highest performance (Fig. 13a and b), indicating that a well-wetted environment facilitates the approach of the reactants to the electrode in the capt-eCO_2R. Based on this observation, Zhang *et al.* used porous Ag foam as an electrode, which showed significantly higher performance than the control carbon cloth as mentioned in Section 2.2.1.[49] Langie *et al.* also constructed an MEA cell using carbon papers that were not treated with PTFE or MPL.[17] To enhance the hydrophilicity of the catalyst and improve CO production, the coral Ag/C was prepared through electrochemical oxidation and reduction processes. The performance of coral Ag/C was compared with Ag nanoparticles, coral Ag, and Ag/C to determine the origin of the high performance associated with the coral Ag/C. They found that the hydrophilicity of the catalyst material, through the transition from Ag nanoparticles to coral Ag and Ag/C structures, along with the measurement of the contact angle with water, contributes significantly to the performance improvement (Fig. 12c and 13c). Additionally, the CO production performance of various carbon papers, both treated and untreated with PTFE, showed a consistent trend where hydrophobic carbon paper resulted in reduced CO production (Fig. 13d).

3.2 Addition of various additives

CO_2 absorbents such as amino-alcohol solutions can interfere with the catalyst surface in the capt-eCO_2R system. As explained in Section 2.1.1, Lee *et al.* observed an increase in performance by adding alkali cation, especially K$^+$, to the monoethanolamine solution, and observed the effect of alkali cation on the composition of electrode surface EDL through Raman spectroscopy and EIS analysis.[24] These results demonstrate that while bulky ammonium cations inhibit reaction rates by preventing the direct transfer of electrons from the cathode to the reactants, this can be overcome by adding alkali cations.

Fink *et al.* confirmed a cation effect similar to that observed in conventional gas-eCO_2R by adjusting the type and concentration of alkali cations in $MHCO_3$ (M = Li, Na, K, Cs) solutions.[58] Furthermore, the influence of the cation on the chemical desorption and electrochemical conversion of CO_2 was investigated. The amount of *in situ* CO_2 was similar regardless of the identity of the cation; however, larger cations increased the CO selectivity, consistent with the known trend of the cation effect. They concluded that solvated alkali cations affect the stabilisation of the reaction intermediate, similar to the gas-eCO_2R.

The organic chains of cationic surfactants are known to inhibit the HER, which competes with the eCO_2R; thus, cationic surfactants have been used as alternative additives to metal cations. Banerjee *et al.* reported that a cationic surfactant suppressed the HER in the gas-eCO_2R by adsorbing onto the surface of the cathode and thereby preventing the approach of water or hydrated cations in the electrolyte.[63] Several similar studies using surfactants have been conducted in the capt-eCO_2R. Lees

10608 | *J. Mater. Chem. A*, 2024, **12**, 10597–10613

This journal is © The Royal Society of Chemistry 2024

Table 4 Structure and properties of the cationic surfactants

Surfactant	Abbreviation	Charge	Counter ion	Structure
Hexadecyl trimethylammonium bromide	CTAB	+	Br^-	
Benzyldimethyl hexadecylammonium chloride	CKC	+	Cl^-	
Sodium dodecyl sulphate	SDS	−	Na^+	
Hexadecyltrimethylammonium chloride	CTAC	+	Cl^-	

et al. added 3 mM CTAB to 3 M $KHCO_3$ to convert captured CO_2 to methane and compared this method to that using a solution without CTAB using a porous copper electrode.[53] The selectivity of the conversion reaction increased from nearly 0% to approximately 30%. In another study, Gutiérrez-Sánchez *et al.* compared the influence of four different surfactants, CTAB, CKC, SDS, and CTAC, on the formate production performance (Table 4) using a Sn wire as a working electrode.[64] In 2 M $KHCO_3$, the 1000 μM of CKC addition resulted in the highest activity, increasing the FE from 12% to 66% at -0.9 V_{RHE}. The aromatic ring of CKC was hypothesised to increase resistance to H^+, thereby improving the FE by more than 20% relative to CTAB, which exhibited the second-best performance.

3.3 Temperature and pressure

During capt-eCO_2R, desorption of CO_2 from the absorption medium is expected to be necessary for electrochemical

conversion into a product. Optimising the physical conditions, such as temperature and pressure, should improve the capt-eCO_2R performance by facilitating the breaking of chemical bonds between the absorbent and CO_2; however, the additional energy required for this process must be considered to ensure overall energy efficiency.

The optimal temperatures vary according to the components and target products of the capt-eCO_2R because temperature affects multiple properties, including the desorption–absorption equilibrium, catalytic reaction rates, and mass transfer. Lee *et al.* adjusted the temperatures of a flow cell system with a Ag catalyst as a cathode.[24] The current density at 60 °C was 15 times higher than at room temperature (RT) and CO FE also increases with temperature (Fig. 14a and b). The additional thermal energy facilitated cleavage of the C–N bond between the amine and CO_2, and accelerated the transfer of reactants. Kim *et al.* studied the effect of temperature in capt-eCO_2R at RT, 40 °C,
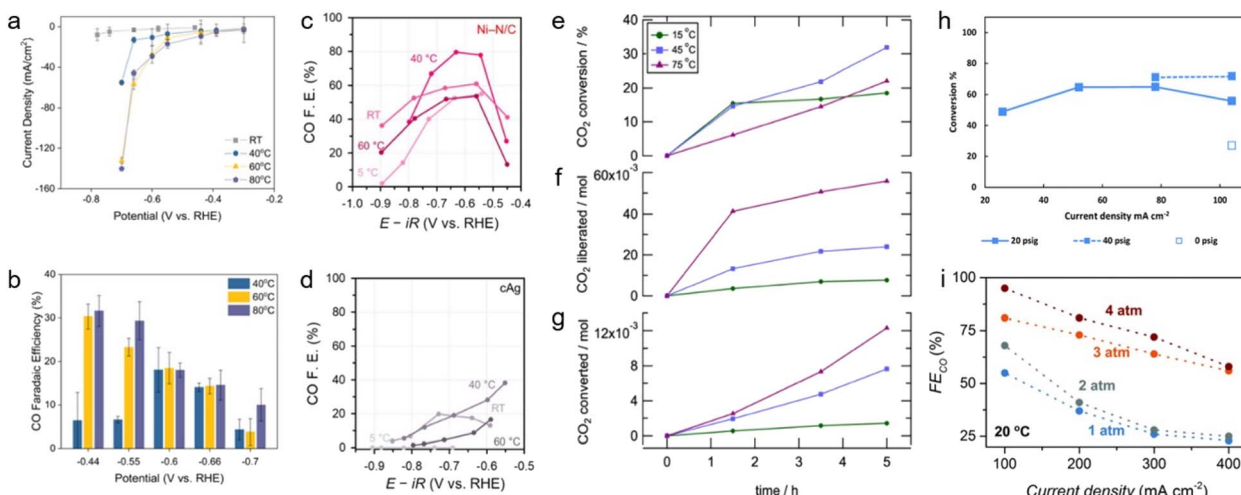

Fig. 14 (a) j–V curve, (b) CO FE of 2 M monoethanolamine with 2 M KCl electrolyte at different temperatures. Copyright 2020,[24] Springer Nature. CO FE of (c) Ni–N/C, and (d) cAg at different temperatures. Copyright 2022,[26] Royal Society of Chemistry. (e) CO_2 conversion, (f) liberated CO_2, and (g) converted CO_2 on a Pb electrode in a 1 M AMP in PC solution as functions of time and temperature. Copyright 2021,[32] American Chemical Society. (h) Conversion profiles of CO_2 released from the CP–H_2CO_3 solution at different current densities and pressures. Copyright 2018,[56] Royal Society of Chemistry. (i) FE_{CO} as a function of pressure at different current densities of Ag foam in 3 M $KHCO_3$. Copyright 2022,[49] Royal Society of Chemistry.

and 60 °C and found that the capt-eCO$_2$R demonstrated peak efficiency at 40 °C (Fig. 14c and d).[26] A higher temperature of 60 °C had positive effects on the desorption of CO$_2$ but also simultaneously accelerated HER; thus, 40 °C was determined to be the optimal temperature for the capt-eCO$_2$R. In addition, Pérez-Gallent *et al.* estimated the CO$_2$ conversion rate, along with the amounts of liberated and converted CO$_2$ at 15 °C, 45 °C, and 75 °C with a Pb electrode in 1 M AMP and PC solution.[32] The highest CO$_2$ liberation and conversion amounts were achieved at 75 °C, demonstrating 8 times higher performance than at 15 °C (Fig. 14f and g). Additionally, the highest CO$_2$ conversion rate was observed at 45 °C (Fig. 14e). While additional thermal energy assists in the desorption and reactions of CO$_2$, the rate of CO$_2$ conversion has an optimal temperature of 45 °C.

Pressure also significantly affects the solubility and reaction rates of gaseous molecules. To understand the effect of pressure effect on capt-eCO$_2$R, Diaz *et al.* measured the CO$_2$ conversion ratio at various pressures of 0, 20, and 40 psig at a current density of −104 mA cm^{-2} in a CHP–H$_2$CO$_3$ mixed solution.[56] The highest CO$_2$ conversion of 71.4% was obtained at 40 psig. High pressure facilitated the redissolution of unreacted CO$_2$ and its participation in the reaction (Fig. 14h). Zhang *et al.* improved the performance on an MEA cell with a porous Ag foam cathode at a constant current density of −100 mA cm^{-2}, by tuning the pressure and temperature.[49] Increasing the temperature from 20 °C to 70 °C increased the CO FE from 59% to 78%, while increasing the pressure from 1 atm to 4 atm increased the CO FE from 55% to 95% (Fig. 14i). Temperature may affect CO$_2$ desorption and mass transfer, whereas increasing the pressure increases the kinetic supply and reaction rate of CO$_2$.

3.4 Other modification

The electrode surface was modified to use the flue gas directly *via* physical separation rather than chemical separation. Al-Attas *et al.* fabricated a permselective GDE composed of a sputtered Ag catalyst on one side and a metal–organic framework (MOF) mixed with Nafion on the other.[65] Owing to its strong ability to physisorb CO$_2$, the MOF called Calgary framework-20 (CALF-20) was used to increase CO$_2$ permselectivity among the multiple gases that make up the flue gas. With the introduction of 10% CO$_2$ into the N$_2$-based gas stream, the permselective GDE showed 95% CO FE while the Ag/PTFE electrode showed only 58% CO FE at −1.32 V$_{RHE}$. CALF-20 showed superior performance in suppressing the oxygen reduction reaction with an oxygen-containing gas stream and improved the wet stability with a wet gas stream.

Kim *et al.* demonstrated that the activity of a given electrode is strongly dependent on the electrolyte composition because it can overcome the interference of the bulky cations typically present in CO$_2$ absorbents.[26] Developing catalyst materials affords control over the EDL and enables the manipulation of PZC of the electrode, which determines the electric field required for ion accumulation under electrocatalytic reaction conditions and tailored the catalyst to be insensitive to the cation species, as explained in Section 2.1.1. Developing catalyst materials is a promising strategy to enhance performance because it can be

implemented into existing systems and circumvents the undesirable side effects of additives such as salt formation.

4. Perspective

The capt-eCO$_2$R system is a promising system that complements the weaknesses of both CO$_2$ capture and CO$_2$ conversion systems. In the field of CO$_2$ capture, capt-eCO$_2$R systems eliminate the requirement for energy-intensive solvent regeneration, gas conditioning, and compression. Concurrently, because the majority of unreacted CO$_2$ remains within the capture medium, eCO$_2$R systems significantly improve the economic feasibility of eCO$_2$R by simplifying or eliminating product separation and recycling process. Although the capt-eCO$_2$R seems a seamless integration of CO$_2$ capture and CO$_2$ conversion, coupled studies considering both reactions thoroughly are essential for developing an advanced, high-performance system.

In the CO$_2$ capture process, the captured CO$_2$ is regenerated by environmental factors such as temperature and pressure. The capt-eCO$_2$R exploits the proton conductivity of the capture medium such that CO$_2$ can be regenerated and activated by pH changes or applied potentials. To date, various CO$_2$ absorbents, such as primary, secondary, and tertiary amine, as well as metal hydroxides, have been preferentially screened as well-known CO$_2$ capture materials, while mixed absorbents or additives have been applied to improve the performance of capt-eCO$_2$R systems. However, in the capt-eCO$_2$R system, the CO$_2$ absorbent acts as both a CO$_2$ absorbent and an electrolyte. Given the active participation of the electrolyte-like cation effect observed in the capt-eCO$_2$R system, further research is required to elucidate the role of the absorbent and identify or develop an ideal absorbent for the capt-eCO$_2$R. In the screening of a promising CO$_2$ absorbent for the capt-eCO$_2$R, we propose to consider multiple properties that specifically address the binding energy and electroconductivity, such as pK_a, molecular structure and size, solvation effect, and charge distribution. An understanding of the effects of these parameters is expected to afford control over the strength of CO$_2$ binding, adsorption, and desorption of the reactants and products, as well as interactions with the catalyst surface. Beyond empirical approaches for selecting a CO$_2$ absorbent, further studies are required to understand the key parameters and their respective impacts.

The electrolyser configuration must also be redesigned to enhance the circulatory efficiency of CO$_2$ absorption, desorption, and conversion. Recent studies commonly employ MEA-type electrolysers for capt-eCO$_2$R systems; however, because MEA electrolysers are designed for use with gas-phase CO$_2$ rather than liquid reactants, the system configuration must be adjusted to ensure their optimal applicability in capt-eCO$_2$R systems. Strongly hydrophobic substrates appear to limit the interaction between the liquid reactant and the catalyst, indicating that superior performance may be achieved using hydrophilic substrates (Section 3.1). This discrepancy may arise from the current designs of the flow path and substrate location, which are optimised for gas delivery. Consequently, a new generation of electrolysers more suitable for liquid reactants is required. In addition, most studies employed carbon

10610 | *J. Mater. Chem. A*, 2024, **12**, 10597–10613

This journal is © The Royal Society of Chemistry 2024

substrates, while other types of substrates remain relatively unexplored.

The selection and development of membranes should be a major focus of future work to improve the performance of the MEA configuration. Current capt-eCO$_2$R systems typically use BPM as a membrane owing to its high H$^+$ and OH$^-$ reflux to each cathode and anode, respectively, which provides sufficient acidity at the cathode side to enable the release and conversion of CO$_2$. The BPM would have been a good choice to ensure good separation, because most previous studies conducted the cathodic and anodic reactions under different electrolyte conditions. However, the structure of the BPM overlaps with those of the CEM and AEM, resulting in a high resistance due to its thickness, where consequently limits the current density that the BPM can provide to approximately 600 mA cm^{-2}.[66] Recent progress in enhancing the performance of the BPM can ensure the longevity of the capt-eCO$_2$R; however, a newly designed or configured electrolyser that does not rely on a BPM should also be considered. Recently, a novel CEM-based system with an interposer was introduced to increase the concentration of *in situ* CO$_2$ at the desired local pH at the catalyst; however, this configuration still requires a high overpotential owing to the presence of an interposer.[55] A new membrane optimised for the capt-eCO$_2$R system should therefore be developed to generate a higher current density and low overpotential.

A thorough understanding of the overall reaction mechanisms could also provide a breakthrough in the development of this system. Opinions regarding the identity of the active species in the capt-eCO$_2$R differ. Some studies have suggested that captured CO$_2$ is reduced directly; however, (bi)carbonate/carbamate are generally considered to be preferentially regenerated to *in situ* CO$_2$ that is then reduced on the catalyst surface. Further reductions to afford the desired products are expected to be similar to those in the gas-eCO$_2$R system; however, this remains to be conclusively demonstrated. Hence, a comprehensive investigation of these mechanisms requires direct observations by *operando*/*in situ* spectroscopy, alongside thermodynamic calculations and multiphysics modeling. Fundamental research in this area can provide valuable insights that inform the development of effective strategies and identify promising approaches.

In the current state of research, significant emphasis has been placed on advancing system development and catalyst engineering to enhance the performance of capt-eCO$_2$R. Given the relatively early stage of development in this field, only a few publications reported on the long-term stability of their system comprehensively.[17,50] To achieve a long-term stable capt-eCO$_2$R system, we may encounter challenges similar to those in conventional gas-eCO$_2$R systems, such as catalyst degradation, membrane stability, and electrolyte changes during prolonged operation. Furthermore, depending on the CO$_2$ absorbent used, different degradation phenomena and their degrees may be expected, necessitating a thorough investigation of the effects of the CO$_2$ absorbent. For instance, with a KOH solution, salt formation on the catalyst surface and flow path is probably unavoidable during extended operation.[38,40,42] Amine-type absorbents may alleviate this issue, but some amines can potentially damage the catalyst and carbon substrate due to their corrosiveness. Moreover, it is essential to consider that catalysts can degrade due to fluctuations in reactant concentration and physical delamination under a liquid reactant circulating system. Therefore, observing the phenomenon of prolonged reactions should be a primary focus, followed by comprehensive studies to address it. All components of the electrochemical system, including the membrane, cathode, anode, and electrolyte, are crucial areas that require further study for long-term stability.

This technology is still in the early stages of research and development; thus, its performance is currently inferior to that of gas-eCO$_2$R technologies. Nevertheless, significant performance improvements are expected over time as the development of the aforementioned component technologies continues to mature, driven by empirical insights gained through gas-CO$_2$R research. In addition, the simplicity of this system will afford economic and environmental benefits that far outstrip those of existing CCUS technologies.

Author contributions

K. L. and G. B. contributed equally to this work, collected and analysed data, and wrote the manuscript. U. L., D. K. L., and C. W. L. contributed to the investigation of recent research trends and wrote the perspective part. Y. J. H. and D. H. W. supervised this study.

Conflicts of interest

The authors declare no competing financial interest.

Acknowledgements

References

1 WMO, *WMO Greenhouse Gas Bulletin (GHG Bulletin) – No. 17: the State of Greenhouse Gases in the Atmosphere Based on Global Observations through 2020*, WMO, 2021.

2 O. Gutiérrez-Sánchez, B. Bohlen, N. Daems, M. Bulut, D. Pant and T. Breugelmans, *ChemElectroChem*, 2022, **9**, e202101540.

3 A. Dubey and A. Arora, *J. Cleaner Prod.*, 2022, **373**, 133932.

4 A. S. Reis Machado and M. Nunes da Ponte, *Curr. Opin. Green Sustainable Chem.*, 2018, **11**, 86–90.

5 G. Y. Duan, X. Q. Li, G. R. Ding, L. J. Han, B. H. Xu and S. J. Zhang, *Angew Chem. Int. Ed. Engl.*, 2022, **61**, e202110657.

6 M. G. Kibria, J. P. Edwards, C. M. Gabardo, C. T. Dinh, A. Seifitokaldani, D. Sinton and E. H. Sargent, *Adv. Mater.*, 2019, **31**, e1807166.

This journal is © The Royal Society of Chemistry 2024

J. Mater. Chem. A, 2024, **12**, 10597–10613 | **10611**

7   C.-T. Dinh, F. P. García de Arquer, D. Sinton and E. H. Sargent, *ACS Energy Lett.*, 2018, **3**, 2835–2840.

8   L. Fan, C. Xia, P. Zhu, Y. Lu and H. Wang, *Nat. Commun.*, 2020, **11**, 3633.

9   B. Zhang, J. Zhang, M. Hua, Q. Wan, Z. Su, X. Tan, L. Liu, F. Zhang, G. Chen, D. Tan, X. Cheng, B. Han, L. Zheng and G. Mo, *J. Am. Chem. Soc.*, 2020, **142**, 13606–13613.

10 T. Jaster, A. Gawel, D. Siegmund, J. Holzmann, H. Lohmann, E. Klemm and U. P. Apfel, *iScience*, 2022, **25**, 104010.

11 P. Yue, Q. Fu, J. Li, X. Zhu and Q. Liao, *Green Chem.*, 2022, **24**, 2927–2936.

12 J. Fernández-González, M. Rumayor, A. Domínguez-Ramos and Á. Irabien, *Int. J. Greenhouse Gas Control*, 2022, **114**, 103549.

13 Y. Hori, H. Konishi, T. Futamura, A. Murata, O. Koga, H. Sakurai and K. Oguma, *Electrochim. Acta*, 2005, **50**, 5354–5369.

14 R. Veneman, *Adsorptive System for Post-combustion CO₂ Capture*, University of Twente, Enschede, 2015.

15 F. Yulia, R. Sofianita, K. Prayogo and N. Nasruddin, *Case Stud. Therm. Eng.*, 2021, **26**, 101093.

16 A. J. Welch, E. Dunn, J. S. DuChene and H. A. Atwater, *ACS Energy Lett.*, 2020, **5**, 940–945.

17 K. M. G. Langie, K. Tak, C. Kim, H. W. Lee, K. Park, D. Kim, W. Jung, C. W. Lee, H.-S. Oh, D. K. Lee, J. H. Koh, B. K. Min, D. H. Won and U. Lee, *Nat. Commun.*, 2022, **13**, 7482.

18 N. S. J. Gao, C. Quiroz-Arita, L. A. Diaz and T. E. Lister, *J. CO2 Util.*, 2021, **43**, 101365.

19 Z. Rastegar and A. Ghaemi, *J. Heat Mass Transf. Res.*, 2021, **58**, 365–381.

20 N. El Hadri, D. V. Quang, E. L. V. Goetheer and M. R. M. Abu Zahra, *Appl. Energy*, 2017, **185**, 1433–1449.

21 D. Fernandes, W. Conway, R. Burns, G. Lawrance, M. Maeder and G. Puxty, *J. Chem. Thermodyn.*, 2012, **54**, 183–191.

22 L. B. Hamdy, C. Goel, J. A. Rudd, A. R. Barron and E. Andreoli, *Mater. Adv.*, 2021, **2**, 5843–5880.

23 B. Yoon, D. C. Calabro, L. S. Baugh, S. Raman and G. S. Hwang, *J. Environ. Chem. Eng.*, 2022, **10**, 108987.

24 G. Lee, Y. C. Li, J.-Y. Kim, T. Peng, D.-H. Nam, A. Sedighian Rasouli, F. Li, M. Luo, A. H. Ip, Y.-C. Joo and E. H. Sargent, *Nat. Energy*, 2020, **6**, 46–53.

25 L. Chen, F. Li, Y. Zhang, C. L. Bentley, M. Horne, A. M. Bond and J. Zhang, *ChemSusChem*, 2017, **10**, 4109–4118.

26 J. H. Kim, H. Jang, G. Bak, W. Choi, H. Yun, E. Lee, D. Kim, J. Kim, S. Y. Lee and Y. J. Hwang, *Energy Environ. Sci.*, 2022, **15**, 4301–4312.

27 M. N. Hossain, S. Ahmad, I. S. da Silva and H. B. Kraatz, *Chemistry*, 2021, **27**, 1346–1355.

28 Y. Qiu, H. Zhong, W. Xu, T. Zhang, X. Li and H. Zhang, *J. Mater. Chem. A*, 2019, **7**, 5453–5462.

29 M. Abdinejad, Z. Mirza, X.-a. Zhang and H.-B. Kraatz, *ACS Sustain. Chem. Eng.*, 2020, **8**, 1715–1720.

30 G. Leverick, E. M. Bernhardt, A. I. Ismail, J. H. Law, A. Arifutzzaman, M. K. Aroua and B. M. Gallant, *ACS Catal.*, 2023, **13**, 12322–12337.

31 M. Bhattacharya, S. Sebghati, Y. M. Vercella and C. T. Saouma, *J. Electrochem. Soc.*, 2020, **167**, 086507.

32 E. Pérez-Gallent, C. Vankani, C. Sánchez-Martínez, A. Anastasopol and E. Goetheer, *Ind. Eng. Chem. Res.*, 2021, **60**, 4269–4278.

33 Y. Matsuzaki, H. Yamada, F. A. Chowdhury, S. Yamamoto and K. Goto, *Ind. Eng. Chem. Res.*, 2019, **58**, 3549–3554.

34 H. M. Stowe and G. S. Hwang, *Phys. Chem. Chem. Phys.*, 2017, **19**, 32116–32124.

35 J. J. Lv, M. Jouny, W. Luc, W. Zhu, J. J. Zhu and F. Jiao, *Adv. Mater.*, 2018, **30**, e1803111.

36 J. Zhang, W. Luo and A. Züttel, *J. Mater. Chem. A*, 2019, **7**, 26285–26292.

37 E. J. Dufek, T. E. Lister and M. E. McIlwain, *Electrochem. Solid-State Lett.*, 2012, **15**, B48.

38 Y. Xu, J. P. Edwards, S. Liu, R. K. Miao, J. E. Huang, C. M. Gabardo, C. P. O'Brien, J. Li, E. H. Sargent and D. Sinton, *ACS Energy Lett.*, 2021, **6**, 809–815.

39 P. Jeanty, C. Scherer, E. Magori, K. Wiesner-Fleischer, O. Hinrichsen and M. Fleischer, *J. CO₂ Util.*, 2018, **24**, 454–462.

40 C. Chen, Y. Li and P. Yang, *Joule*, 2021, **5**, 737–742.

41 C. M. Gabardo, C. P. O'Brien, J. P. Edwards, C. McCallum, Y. Xu, C.-T. Dinh, J. Li, E. H. Sargent and D. Sinton, *Joule*, 2019, **3**, 2777–2791.

42 S. Popovic, M. Smiljanic, P. Jovanovic, J. Vavra, R. Buonsanti and N. Hodnik, *Angew Chem. Int. Ed. Engl.*, 2020, **59**, 14736–14746.

43 F. Li, Y. C. Li, Z. Wang, J. Li, D.-H. Nam, Y. Lum, M. Luo, X. Wang, A. Ozden, S.-F. Hung, B. Chen, Y. Wang, J. Wicks, Y. Xu, Y. Li, C. M. Gabardo, C.-T. Dinh, Y. Wang, T.-T. Zhuang, D. Sinton and E. H. Sargent, *Nat. Catal.*, 2019, **3**, 75–82.

44 E. S. Sanz-Perez, C. R. Murdock, S. A. Didas and C. W. Jones, *Chem. Rev.*, 2016, **116**, 11840–11876.

45 X. Min and M. W. Kanan, *J. Am. Chem. Soc.*, 2015, **137**, 4701–4708.

46 Y. Hori and S. Suzuki, *J. Electrochem. Soc.*, 1983, **130**, 2387.

47 T. Li, E. W. Lees, M. Goldman, D. A. Salvatore, D. M. Weekes and C. P. Berlinguette, *Joule*, 2019, **3**, 1487–1497.

48 E. W. Lees, J. C. Bui, D. Song, A. Z. Weber and C. P. Berlinguette, *ACS Energy Lett.*, 2022, **7**, 834–842.

49 Z. Zhang, E. W. Lees, F. Habibzadeh, D. A. Salvatore, S. Ren, G. L. Simpson, D. G. Wheeler, A. Liu and C. P. Berlinguette, *Energy Environ. Sci.*, 2022, **15**, 705–713.

50 Y. G. C. Li, G. Lee, T. G. Yuan, Y. Wang, D. H. Nam, Z. Y. Wang, F. P. G. de Arquer, Y. Lum, C. T. Dinh, O. Voznyy and E. H. Sargent, *ACS Energy Lett.*, 2019, **4**, 1427–1431.

51 A. Bonet Navarro, A. Nogalska and R. Garcia-Valls, *Electrochem*, 2021, **2**, 64–70.

52 T. Li, E. W. Lees, Z. Zhang and C. P. Berlinguette, *ACS Energy Lett.*, 2020, **5**, 2624–2630.

53 E. W. Lees, A. Liu, J. C. Bui, S. Ren, A. Z. Weber and C. P. Berlinguette, *ACS Energy Lett.*, 2022, **7**, 1712–1718.

54 J. Lee, H. Liu and W. Li, *ChemSusChem*, 2022, **15**, e202201329.

55 G. Lee, A. S. Rasouli, B.-H. Lee, J. Zhang, D. H. Won, Y. C. Xiao, J. P. Edwards, M. G. Lee, E. D. Jung,

10612 | *J. Mater. Chem. A*, 2024, **12**, 10597–10613

This journal is © The Royal Society of Chemistry 2024

F. Arabyarmohammadi, H. Liu, I. Grigioni, J. Abed, T. Alkayyali, S. Liu, K. Xie, R. K. Miao, S. Park, R. Dorakhan, Y. Zhao, C. P. O'Brien, Z. Chen, D. Sinton and E. Sargent, *Joule*, 2023, **7**, 1277–1288.

56 L. A. Diaz, N. Gao, B. Adhikari, T. E. Lister, E. J. Dufek and A. D. Wilson, *Green Chem.*, 2018, **20**, 620–626.

57 S. Hosseini, H. Moghaddas, S. Masoudi Soltani, M. K. Aroua, S. Kheawhom and R. Yusoff, *J. Environ. Chem. Eng.*, 2018, **6**, 6335–6343.

58 A. G. Fink, E. W. Lees, Z. Zhang, S. Ren, R. S. Delima and C. P. Berlinguette, *ChemElectroChem*, 2021, **8**, 2094–2100.

59 E. W. Lees, M. Goldman, A. G. Fink, D. J. Dvorak, D. A. Salvatore, Z. Zhang, N. W. X. Loo and C. P. Berlinguette, *ACS Energy Lett.*, 2020, **5**, 2165–2173.

60 M. D. Gálvez-Vázquez, P. Moreno-García, H. Xu, Y. H. Hou, H. F. Hu, I. Z. Montiel, A. V. Rudnev, S. Alinejad, V. Grozovski, B. J. Wiley, M. Arenz and P. Broekmann, *ACS Catal.*, 2020, **10**, 13096–13108.

61 S. Verma, Y. Hamasaki, C. Kim, W. Huang, S. Lu, H.-R. M. Jhong, A. A. Gewirth, T. Fujigaya, N. Nakashima and P. J. A. Kenis, *ACS Energy Lett.*, 2017, **3**, 193–198.

62 M. E. Leonard, L. E. Clarke, A. Forner-Cuenca, S. M. Brown and F. R. Brushett, *ChemSusChem*, 2020, **13**, 400–411.

63 S. Banerjee, X. Han and V. S. Thoi, *ACS Catal.*, 2019, **9**, 5631–5637.

64 O. Gutiérrez-Sánchez, N. Daems, W. Offermans, Y. Y. Birdja, M. Bulut, D. Pant and T. Breugelmans, *J. CO2 Util.*, 2021, **48**, 101521.

65 T. Al-Attas, S. NabilK, A. S. Zeraati, H. S. Shiran, T. Alkayyali, M. Zargartalebi, T. Tran, N. N. Marei, M. A. Al Bari, H. Lin, S. Roy, P. M. Ajayan, D. Sinton, G. Shimizu and M. G. Kibria, *ACS Energy Lett.*, 2022, **8**, 107–115.

66 C. Shen, R. Wycisk and P. N. Pintauro, *Energy Environ. Sci.*, 2017, **10**, 1435–1442.

This journal is © The Royal Society of Chemistry 2024

J. Mater. Chem. A, 2024, **12**, 10597–10613 | **10613**